Polarized second-harmonic generation with broadband femtosecond pulses

Brian K. Canfield, Kaisa Laiho, and Martti Kauranen

Institute of Physics, Optics Laboratory, Tampere University of Technology, P. O. Box 692, FI-33101 Tampere, Finland

Received October 12, 2006; accepted December 11, 2006;
posted January 16, 2007 (Doc. ID 75912); published April 17, 2007

We computationally investigate polarized second-harmonic generation (SHG) of a spectrally broad femtosecond pulse following transmission through traditional quarter wave plates (QWPs). Because the sideband modes of a broadband pulse can interact through sum-frequency generation processes, the SHG responses for several experimentally relevant cases exhibit asymmetries between individual sideband modes, spectral peak shifts, and, critically, artificial chiral signatures. Remarkably, errors in the various sum-frequency sidebands are found to compensate for each other so that the total SHG response approaches the ideal narrowband response. This occurs in the absence of significant axis misalignment in a compound QWP. Hence, our results suggest that polarized femtosecond SHG can be remarkably tolerant against the broad bandwidth of ultrashort pulses.

OCIS codes: 190.7110, 190.2620, 260.5430, 320.5550.

1. INTRODUCTION

The use of ultrashort pulses in optical measurements is opening new realms of physical phenomena regarding light–matter interactions for investigation. Femtosecond (fs) pulses have provided the ability to probe molecular chemical reactions, excited state evolution, and cis-trans isomerization in real time with time-resolved spectroscopy.[1] Ultrashort pulses also offer extremely high peak power densities, an advantageous attribute from the viewpoint of nonlinear optical phenomena, such as the generation of high-order harmonics.[2] High repetition rates coupled with short-pulse durations impart low energies per pulse, which can also be particularly useful for nonlinear optical studies of fragile samples, such as biological matter and highly absorbing dyes. Metal nanostructures are at present another fragile system of particular interest. Although even fs pulses may cause irreversible material changes in metallic nanoparticles,[3–5] nondamaging nonlinear optical measurements can also be performed.[6–8] Hence, ultrashort laser pulses occupy a strategic niche in nonlinear photonics research.

Traditional pulsed laser sources, such as nanosecond (ns) Nd:YAG and picosecond (ps) dye lasers, have comparatively long-pulse durations with narrow spectral bandwidths (BWs) of less than 1 nm. Thus, it is often justified to treat their optical fields as having a single frequency. In the sub-ps regime, on the other hand, the field consists of a large number of oscillating modes, and short-pulse laser operation is usually attained by mode locking.[9] The presence of these additional modes complicates nonlinear optical processes, because the sideband modes can behave differently, and their contributions to the nonlinear response have to be treated separately.[10]

The broadband (BB) nature of fs pulses also has significant consequences for second-harmonic generation (SHG). Because of the broadness of the fundamental spectrum, group-velocity dispersion restricts the nonlinear frequency conversion region to thin systems. Distribution of the pulse energy into sidebands further hampers conversion efficiency, necessitating phase- and/or group-velocity matching schemes to increase the SHG output.[11–14] In BB-SHG, the sidebands contribute to the total SHG response by coupling through sum-frequency generation[15–17] (SFG).

BB frequency conversion has been considered from various approaches.[18–24] However, because of its tensor nature, SHG is highly sensitive to the state of polarization,[25] a facet that has often been overlooked in these studies, although a few polarized BB-SHG and SFG measurements have been reported.[26–28] The behavior of polarization-control optics with BB pulses is thus a vital concern. Calcite laser polarizers are natural BB linear polarizers, although poorly cut or aligned crystals proscribe good linear polarization.[29] Retardation optics such as wave plates (WPs), on the other hand, are normally designed for a single wavelength centered within a limited spectral acceptance range specified by the tolerance, over which the deviation from nominal retardation falls within certain limits. Tolerances for commonly used crystal quartz WPs, for instance, correspond to ranges of just a few nm,[30] making them dubious choices for dealing with spectrally broad, ultrashort pulses.

Moreover, WPs may contain certain errors and defects that detrimentally affect the polarization, such as misaligned crystal, elliptical axes, retardation that varies across the clear aperture, or even partially polarizing WPs.[29,31,32] WP properties have thus also received their share of attention.[29,33–35] The basic message is that one should not simply rely on manufacturers' specifications and instead always test any new optic to verify its behavior before use in experiments where precise performance is required.

A quarter-wave plate (QWP) is often used to achieve circular polarization (CP) states, which are important for certain optical characterization techniques, both linear and nonlinear.[35–38] Circular dichroism in the SHG response (SHCD), or a difference in SHG efficiency between the two CP states (left and right), is a basic measure of chirality.[36,37] High-quality polarization is required in these measurements, so understanding the limitations of a QWP is vital. A crystal axis misalignment, for instance, means that true CP is unattainable, even for a monochromatic source; the transmitted polarization will always retain some ellipticity because such a misaligned optic does not possess well-defined principal axes.[39] However, the question of how typical narrowband retardation optics affect the polarization of spectrally broad fs pulses and their subsequent effects on BB-SHG has not been treated in detail.

In this paper, we examine numerically the performance of a traditional crystal quartz QWP illuminated by a BB fs pulse. The pulse is approximated by multiple, closely spaced discrete modes, and the retardation and final polarization state of each mode exiting the QWP is determined from the birefringence of quartz and the thickness of the QWP. Dispersion of the birefringence is included in the calculation. Increasing the thickness (i.e., a multiorder QWP) severely restricts the spectral acceptance range of the QWP. Crystal axis misalignment in a homogeneous compound (two-crystal) QWP further complicates the resulting pulse polarization.

The second-order response is investigated by modeling several experimentally relevant cases, including achiral rodlike molecules and an intentionally chiral sample. The samples are assumed to be thin so that phase-matching considerations and group-velocity dispersion can be neglected. Despite the deviations in the fundamental pulse polarization, distortions in the individual sidebands of the SHG field are found to compensate for each other, causing the total SHG response to approach more closely—provided the pulse BW is not too great—the ideal response of a true zero-order QWP with a narrowband source. Deviations occur in the sidebands even with a true zero-order QWP, but through sideband compensation the total SHG response with a true zero-order QWP is found to reproduce the ideal response. However, effective compensation is also startlingly demonstrated for a moderate BW with a multiorder QWP. For a larger BW, though, compensation no longer balances distortion and the total SHG response of the multiorder QWP can deviate substantially from ideal. Also of considerable import is the fact that a crystal misalignment in a compound QWP can introduce an artifical chiral signature to an achiral sample, which may have significant experimental consequences. Interestingly, increasing the thickness of the compound QWP can nearly eliminate the artifical chiral signature, implying that dispersion also plays a role in helping compensate for polarization distortions in the total SHG response.

2. PULSE PROPAGATION THROUGH A RETARDER

The nominal spectral acceptance range of a WP can be determined from the specified retardation tolerance and is typically in the range of $\lambda/500$ to $\lambda/200$.[30] For example, if $\lambda_0 = 1060$ nm, a zero-order QWP with tolerance $\lambda/500$ yields a range of just ±9 nm. However, the BW of moderately short fs pulses can extend tens of nm, which clearly exceeds the range of a typical WP. The question of how a WP handles such broad pulses then becomes extremely important for measurements where precise polarization control is necessary.

To understand the behavior of a WP with spectrally broad pulses, we must propagate the pulse through the WP and account for phase and polarization modifications. To develop a basic understanding as to how the broad BW associated with short pulses influences the polarization properties, we use a simplified approach where group-velocity dispersion through the WP (pulse chirp) is disregarded. The task is easily addressed as a matrix equation of the form $\mathbf{p}' = M\mathbf{p}$, where $\mathbf{p}$ and $\mathbf{p}'$ are the input and output polarizations in the laboratory frame, respectively, and M is the system matrix that accounts for the changes effected by the WP.

In the laboratory frame, $\hat{\mathbf{p}}$ and $\hat{\mathbf{s}}$ designate, respectively, the axes parallel and perpendicular to the plane of incidence, and the propagation direction; the laboratory $\mathbf{Z}$ axis coincides with the WP $\mathbf{z}$ axis, as depicted in Fig. 1. For a WP oriented at an arbitrary angle θ about the $\mathbf{z}$ axis, the components of the input polarization must first be projected into the WP coordinate system. This is accomplished through the standard rotation matrix, $R(\theta)$[40]:

$$R(\theta) = \begin{bmatrix} \cos(\theta) & \sin(\theta) \\ -\sin(\theta) & \cos(\theta) \end{bmatrix}. \tag{1}$$

The phase gained by each polarization component through the WP depends on the birefringence and thickness (optical path difference) of the WP material. The birefringence and dispersion are specified by $\Delta n(\lambda) = n_e(\lambda) - n_o(\lambda)$, where $n_o(\lambda)$ ($\hat{\mathbf{o}}$) and $n_e(\lambda)$ ($\hat{\mathbf{e}}$) are the ordinary and extraordinary refractive indices, respectively. If the thickness of the crystal is d, then upon propagation through it the phase of each component is modified according to[40]

$$W = \begin{bmatrix} e^{i(2\pi/\lambda)n_o(\lambda)d} & 0 \\ 0 & e^{i(2\pi/\lambda)n_e(\lambda)d} \end{bmatrix}. \tag{2}$$

The retardation by a compound WP consisting of two homogeneous crystals is given by $\rho(\lambda) = 2\pi\Delta n(\lambda)\Delta d/\lambda$,

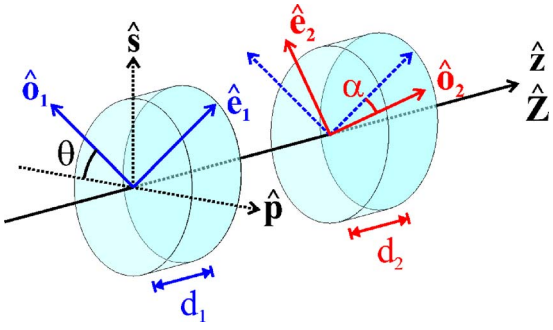

Fig. 1. (Color online) Structure of a compound WP with a misalignment α between the axes of the two crystals. Distances along $\hat{\mathbf{z}}$ are greatly exaggerated for illustrative purposes.

where $\Delta d = d_2 - d_1$ is the thickness difference between the two crystals.[40] For a QWP, $\rho = \pi/2$. Thus, the overall thickness of a compound WP is ideally unimportant, at least for monochromatic inputs. However, dispersion in thicker WPs becomes significant for BB sources.

If an angular misalignment, α, between the crystal axes in a compound WP is introduced (Fig. 1), the polarization transmitted by crystal 1 must then be projected into the rotated axes of crystal 2 with $R(\alpha)$ before the next phase modification is carried out.[32] As the final propagation step, the output polarization must be projected back into the laboratory frame. Thus, the system matrix describing the polarization transmitted by a compound WP is given by

$$M = R(-\theta)R(-\alpha)W_2R(\alpha)W_1R(\theta). \tag{3}$$

For a single-crystal WP, the product $R(-\alpha)W_2R(\alpha)$ is simply removed to obtain the appropriate system matrix.

3. BROADBAND SECOND-HARMONIC GENERATION

A real fs pulse contains a very large number of discrete, equally spaced frequency modes. Consider a short pulse centered at $\lambda_0 = 1\ \mu$m with a spectral BW $\Delta\lambda = 20$ nm. If we assume an air-filled laser cavity of length $L = 1$ m, the number of modes, N, contained in the pulse is given by[9]

$$N = \frac{2L\Delta\lambda}{\lambda_0^2} = 40{,}000. \tag{4}$$

It is computationally infeasible to address this entire spectrum. However, the mode spacing is less than 10^{-3} nm, so the spectrum can be reasonably approximated as continuous. By describing a spectral band centered at $\lambda_0 = 1060$ with $\sim 10^3$ modes (mode spacing of ≈ 0.03 nm), we can again legitimately discretize this continuous spectrum to make a more tractable problem for calculation purposes. Because the modes are evenly distributed in the frequency domain but not in the wavelength domain, it is thus necessary to perform the calculations in the frequency domain. [However, the frequency terms ω_0 and $2\omega_0$ are commonly interchanged with the fundamental and second-harmonic (SH) wavelength terms, and in view of the following calculations it is therefore convenient to adopt this nomenclature for discussing the results, except where explicit reference to wavelength is more appropriate.]

Our fundamental pulse thus consists of 10^3 evenly spaced frequency modes distributed symmetrically about the central frequency with a BW specified by the full width at half maximum (FWHM). The mode spacing is made a function of the FWHM in order to maintain the number of modes for any pulse width. The total spectral distribution of the fundamental pulse extends to either side of ω_0 by $4\times$FWHM, and the spectral intensity at the edges of the pulse is $<0.5\%$ of the maximum at ω_0, ensuring that the full sideband distributions of the fundamental pulse are taken into account.

The central experimental configuration investigated in this work is depicted in Fig. 2. The configuration corresponds to an actual experimental setup for single-beam

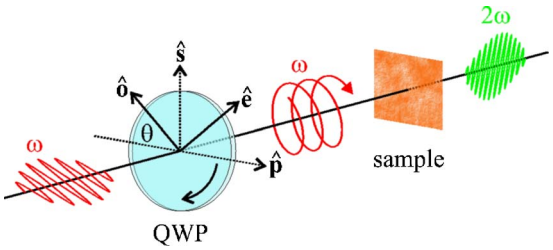

Fig. 2. (Color online) Core configuration of a BB-SHG experiment.

continuous polarization variation measurements with SHG.[41] For all calculations, the input fundamental pulse is always linearly polarized along $\hat{\mathbf{p}}$. According to its design parameters and rotation angle θ, the QWP transmits the fundamental pulse with a specific modified polarization, which then undergoes frequency conversion in the sample through SHG and SFG processes. We apply a simplified conversion scheme in which the sample is assumed to be thin compared with the coherence length. Propagation of the fields within the sample, depletion of the fundamental beam, and phase-matching and group-velocity dispersion issues can thus be neglected.[25]

We need to determine the response electric field at the SH frequency for a given polarization. We describe the fundamental pulse as a plane-wave packet with discrete frequency modes ω propagating in the $\hat{\mathbf{z}}$ direction. The fundamental field of mode ω at a given position z is expressed by $E(\omega) = A(\omega)\mathbf{p}(\omega)$, where $A(\omega)$ represents the complex scalar amplitude and $\mathbf{p}(\omega)$ is the optical polarization obtained in Section 2.

The upconversion of two fundamental field frequency components at ω_1 and ω_2 yields a response field at the sum frequency $\Omega = \omega_1 + \omega_2$, such that $E(\Omega) \propto E(\omega_1)E(\omega_2)$.[25] For a monochromatic source operating at $\omega_1 = \omega_2 \equiv \omega_0$, SHG occurs at $\Omega = 2\omega_0$. However, with a BB pulse we also must consider the sum-frequency contributions from the sideband modes $\omega_1 \neq \omega_2$ to the total SHG response. We can rewrite $\omega_2 = \Omega - \omega_1$ and substitute this into the expression for $E(\omega_2)$. If the field magnitudes are normalized, we can introduce expansion coefficients to account for all the possible polarization combinations[37] and then sum over all modes ω_1 that result in SFG and SHG contributions to the polarized ($i = p, s$) response field at Ω:

$$E_i(\Omega) = \sum_{\omega_1} [f_i E_p(\omega_1)E_p(\Omega - \omega_1) + g_i E_s(\omega_1)E_s(\Omega - \omega_1) + h_i E_p(\omega_1)E_s(\Omega - \omega_1)]. \tag{5}$$

The complex coefficients f_i, g_i, and h_i depend in general on frequency, but here we will assume that their dispersion is negligible over the pulse BW. Expressed in this way, the response field in Eq. (5) appears as a discretized convolution.[42,43] From this point, it is straightforward to calculate the spectral intensity from $I_i(\Omega) = |E_i(\Omega)|^2$. Assuming the detector is slow compared with the pulse duration to avoid frequency beating, the total SHG response is obtained from the sum of the spectral intensities, $I_i = \Sigma_\Omega I_i(\Omega)$.

4. POLARIZATION IN THE LINEAR RESPONSE

The shorter the pulse duration, the wider its BW becomes. We can relate the pulse's temporal length, Δt, to $\Delta\lambda$ by[9]

$$\Delta\lambda = \frac{\beta\lambda_0^2}{c\Delta t}, \tag{6}$$

where β is the time-bandwidth product, a numerical factor that arises from the uncertainty constraint of Fourier theory (β=0.315 for a transform-limited sech^2 pulse or 0.441 for a Gaussian pulse), and c is the speed of light. We have chosen to model a sech^2 pulse, a shape typical of fs laser pulses. Four different BWs centered at λ_0 =1060 nm were selected, representing a wide range of typical pulse lengths reported (Table 1). Note that BW1 corresponds to a traditional narrowband (quasi-monochromatic) ps source.

Several QWP configurations were investigated. All calculations model a QWP comprised of crystal quartz, a common birefringent WP material whose dispersion is well known.[44] The basic parameters are listed in Table 2. QWPT represents a true zero-order (single-crystal) retarder and multiorder QWPM is also a single-crystal retarder of order 8, both of whose thicknesses are determined from the birefringence of crystal quartz at the central wavelength of 1060 nm and the retardation $\rho(\lambda_0)$.

The nominal thickness of quartz QWPs is listed as 1.0–2.5 mm.[30] We therefore examined three different overall thicknesses in this range (Table 2) with compound zero-order QWPC, where Δd is simply equal to the thickness of QWPT. A perfectly aligned QWPC is thus equivalent to QWPT regardless of d, but with QWPC we must also consider an additional complication: an axial misalignment between the two crystals. Misalignments of α =0.1°–5° between the crystals were also studied. The retardation properties of a misaligned compound quartz QWP with a BB, continuous-wave source have been addressed previously, but the responses of single-crystal QWPs were neglected.[32] In our work, we also focus on the BB-SHG response and how it is affected by polarization errors. Elliptical QWP axes were not modeled, although they may be another common but overlooked source of polarization error.[29]

Table 1. Spectral BWs ($\Delta\lambda$) and Equivalent Durations (Δt) Studied

Pulse	$\Delta\lambda$ (nm)	Δt (fs)
BW1	0.1	10^4
BW2	6	200
BW3	25	50
BW4	120	10

Table 2. Basic QWP Configurations[a]

QWP	Type	d (mm)	Range (nm)
T	True zero	0.030	1009–1117
M	Multiorder 8	1.005	1058–1062
C	Compound zero	1.0, 1.5, 2.0	1009–1117

[a]The intended operation wavelength (ω_0) is 1060 nm in all cases.

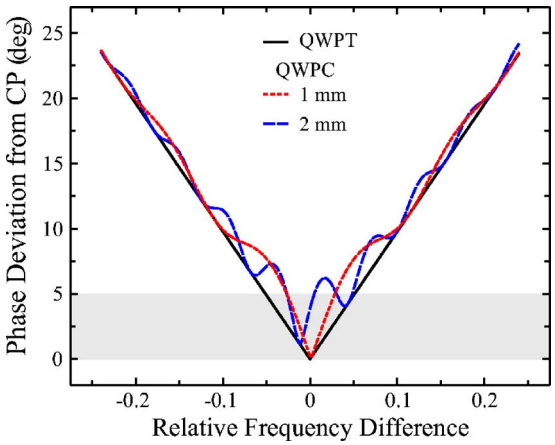

Fig. 3. (Color online) Phase deviations from CP (90°) for QWPT and 3°-misaligned QWPC for thicknesses of 1 and 2 mm. The shaded region indicates the 5° tolerance condition.

The spectral acceptance range of each QWP (Table 2) is determined by the phase deviation between the polarization state transmitted by the QWP when set to pass CP (i.e., θ=±45° in Fig. 2) and the ideal quarter-wave retardation of 90°, because this QWP orientation effectively yields the maximum modification of the input polarization state. The allowed phase deviation is ≤5°, corresponding to a relaxed retardation tolerance of $\lambda/72$. Both the true zero-order QWPT and aligned QWPC accept a very wide range of 108 nm under this tolerance, so they are certainly applicable to longer fs pulses. However, there is a limit to the pulse width that even QWPT can pass within tolerance: for a pulse BW smaller than 26 nm (pulse duration longer than 45 fs), the phase deviation of the entire pulse BW just falls within the 5° criterion, but for greater BWs (i.e., shorter pulses), the phase deviation begins to exceed the tolerance at the sideband edges. Of course, the tighter the tolerance applied, the narrower the range will be: for the manufacturer-specified retardation tolerance of $\lambda/500$, the acceptance range of QWPT is a mere 16 nm (75 fs). The much larger phase difference accumulated through the thicker multiorder QWPM severely restricts its nominal usage range to just 3 nm(~400 fs). Actually, QWPM exhibits multiple widely separated narrow bands distributed across the entire fundamental spectrum (e.g., the nearest neighboring bands are 1003–1005 and 1121–1124 nm).

The overall thickness of an aligned QWPC has no effect on its range; it behaves exactly like QWPT, as expected. However, crystal misalignment has serious consequences for the transmitted polarization,[32] and thickness can thus become a sensitive factor. Figure 3 shows the phase deviations as a function of the frequency relative to ω_0 for a 3° crystal misalignment in the minimum- and maximum-thickness QWPCs, as compared to the reference QWPT. Misalignment introduces oscillatory behavior to the polarization phase. Note also that the minimum phase deviation location shifts away from the central frequency with increasing thickness. This shift results from the

phase differences accumulated through the thicker, dispersive crystals of QWPC. It is possible that the range can shift so far that the QWP will no longer even operate properly at ω_0. Indeed, for the 2 mm QWPC, the minimum deviation occurs at 1072 nm (range of 1055–1089 nm), which means that pulses centered at 1060 nm will never achieve high-quality CP at ω_0. However, even with a misalignment of $\alpha=5°$ in a 1 mm QWPC, the minimum shifts just 1 nm, although the range is considerably restricted (1041–1078 nm).

The combined effects of misalignment and thickness in QWPC also lead to acceptance range splitting as with QWPM. For a misalignment angle of $\alpha=2.4°$ in the 2 mm QWPC, the usable range begins to split apart at approximately 1041 nm. A 4° misalignment shifts the range so that ω_0 no longer lies within it. However, for the 1 and 1.5 mm versions, the range remains intact at approximately ω_0, although it shrinks from the shorter-wavelength end while the minimum deviation shifts toward longer wavelengths. This suggests that the thinner the QWP, the better. True zero order is best, as may be expected, but a QWPC of 1 mm or less does not appear to be very sensitive in the case of small misalignments.

Another way to illustrate the deviation of Fig. 3 is through the eccentricity, ϵ, of the polarization, obtained from the ratio of the semiminor axis, b, to the semimajor axis, a (Ref. 45):

$$\epsilon = \sqrt{1-\left(\frac{b}{a}\right)^2}. \tag{7}$$

Note that the value of ϵ lies between 0 (CP) and 1 (linear polarization). Figure 4 displays ϵ for QWPT and several misaligned angles of the 1 mm QWPC. The oscillations resulting from misalignment indicate that the polarization azimuth direction also varies throughout the sidebands. To emphasize this variation, we have chosen to apply a sign convention to ϵ based on the orientation of the polarization ellipse, ψ, defined as the angle between a and the p axis.[40] The convention is such that $\epsilon>0$ indicates that the projection of a is greater along $\hat{\mathbf{p}}$, while $\epsilon<0$ means that a is more closely aligned to $\hat{\mathbf{s}}$, corresponding to Fig. 5.

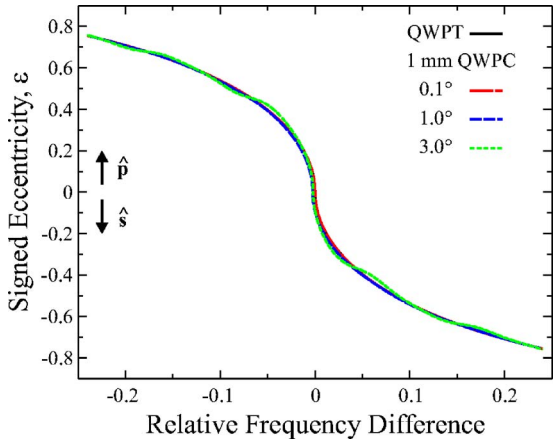

Fig. 4. (Color online) Signed eccentricity of the polarization for QWPT and 1 mm thick QWPC with misalignments of 0.1°, 1°, and 3°. The sign of ϵ indicates whether the projection of a is greater along $\hat{\mathbf{p}}$ (positive) or $\hat{\mathbf{s}}$ (negative) in Fig. 5.

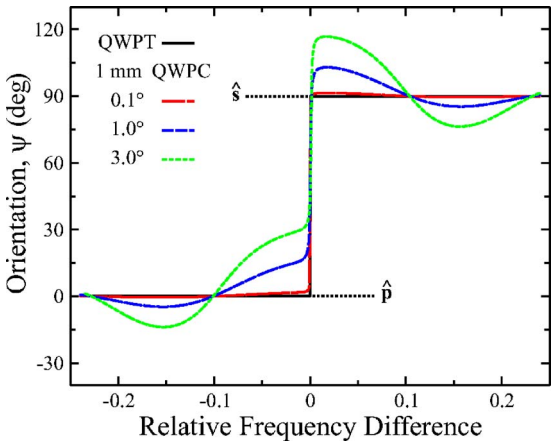

Fig. 5. (Color online) Polarization ellipse orientation for the QWP configurations in Fig. 4.

For all cases in Fig. 4, the extreme edges of the sidebands approach linear polarization, and approximate CP occurs only very near ω_0. A thicker, misaligned QWPC results in more frequent oscillations, but even with QWPT, the transmitted polarization varies strongly throughout the pulse spectrum.

As Fig. 5 shows, the polarization ellipse is oriented differently in the sidebands. For QWPT, the polarization at ω_0 is circular, but moving into the lower sideband causes the polarization to become slightly elliptical and oriented along $\hat{\mathbf{p}}$. In the upper sideband, however, the ellipse is oriented along $\hat{\mathbf{s}}$, resulting in the discontinuous step through ω_0. The orientation remains constant throughout each sideband, though, which means that the phase difference between the individual p and s components depends linearly on frequency. However, the misalignment-induced fluctuations in the polarization direction of QWPC mean that the phase difference here no longer depends linearly on frequency. This may, in turn, result in reduced SHG efficiency, because harmonic generation efficiency has been shown to depend on the ellipticity of the polarization.[46] The distortion worsens with both increased misalignment angle and QWP thickness, but for small misalignments in a thin QWP the retardation of each frequency mode is not significantly affected. No misalignment is, of course, best; but if one exists, it should be less than $\alpha=0.5°$ to avoid significant distortion.

5. POLARIZATION IN THE SECOND-ORDER RESPONSE

We now proceed to examine in detail the SHG responses resulting from the modified polarizations discussed in the previous section. Three variations of the coefficients *fgh* from Eq. (5) were selected, representing realistic experimental samples (Table 3). Set S1 corresponds to the detection of an *s*-polarized SHG signal from an isotropic surface or thin film. Set S2 describes an isotropic thin film of one-dimensional rodike molecules using *p*-polarized detection.[47] S3 intentionally generates a chiral signature, an SHCD response, through the phase shift introduced by the small imaginary *f*.

First, we consider the multiorder QWPM. Figure 6 depicts the SHG responses for the chiral set S3, BW3 at the

central SHG frequency $2\omega_0$ and in the sidebands at $\pm\frac{1}{2}$ FWHM of the SHG spectrum. Because its acceptance range is so small, QWPM strongly distorts the polarization of the fundamental pulse, resulting in unusual, asymmetric SHG responses at the individual frequencies. However, by accounting for all contributions to the total SHG response, we discover an astonishing result: the sidebands compensate for each other, as seen in the excellent agreement with the reference response generated with QWPT and BW1, shown in Fig. 7. Sideband compensation occurs provided the pulse BW does not exceed QWPM's range too greatly. For the very wide BW4, the sideband compensation is no longer effective and the SHCD is almost completely eliminated in Fig. 7. The degree of compensation also depends on the sample conditions specified by *fgh*. Set S1 is relatively insensitive to BW and shows good compensation even for BW4, although some slight asymmetry appears near the CP states. With set S2, on the other hand, the magnitude of the deviation around the CP states grows with increasing BW.

Table 3. Coefficient Sets from Eq. (5) Studied

Set	*f*	*g*	*h*
S1	0	0	1
S2	1	0.33	0
S3	0.1i	0	1

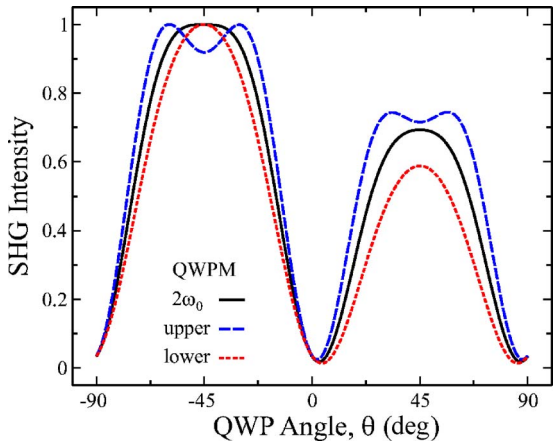

Fig. 6. (Color online) Normalized SHG responses at $2\omega_0$ and in the sidebands generated from coefficient set S3 with QWPM, BW3.

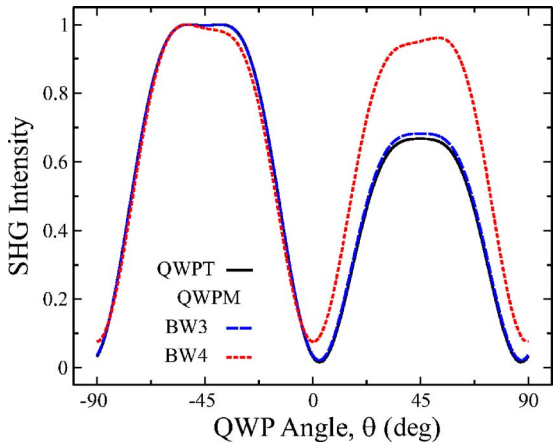

Fig. 7. (Color online) Normalized total SHG responses generated from coefficient set S3 with QWPT, BW1 and QWPM, BW3, and BW4.

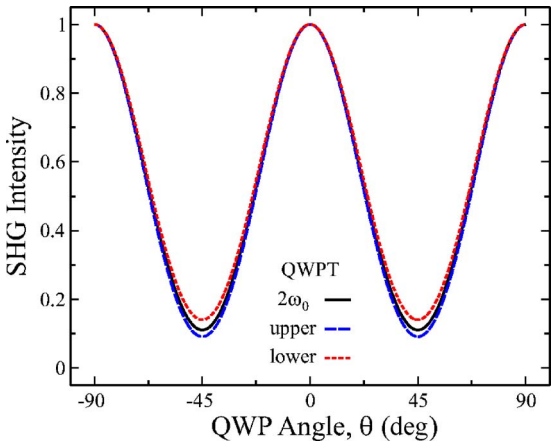

Fig. 8. (Color online) Normalized SHG responses at $2\omega_0$ and in the sidebands generated from coefficient set S2 with QWPT, BW4.

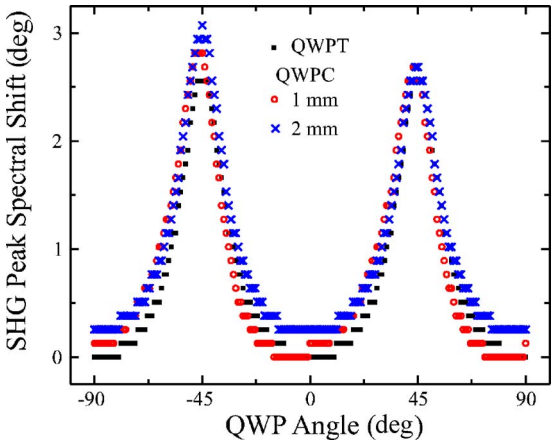

Fig. 9. (Color online) Spectral shift of the SHG peak generated from coefficient set S2, BW4 with QWPT and 1°-misaligned QWPC for thicknesses of 1 and 2 mm.

Deviations in the sidebands occur for large BWs even with QWPT, although the deviations are small compared to QWPM. Set S2, shown in Fig. 8, evinces the greatest difference between the sideband responses. However, full sideband compensation occurs for all coefficient sets with QWPT, even with BW4, yielding essentially exact duplicates of the references obtained with BW1. The behavior of misaligned QWPC appears similar to QWPT, but differs in detail: The magnitudes of the sideband deviations are larger for all sets, and a small angular phase shift also occurs, compared with QWPT. This would affect fitting analysis by yielding different *fgh* values.[36,37]

If the fundamental pulse BW exceeds the acceptance range of the QWP, the SHG spectral peak can shift away from $2\omega_0$, even with QWPT, as Fig. 9 depicts for set S2. This shift results from different sideband modes preferen-

tially coupling to the *fgh* coefficients. Misalignment in QWPC again introduces asymmetry to the response, with differing shifts between the two nominal CP locations at $\theta = \pm 45°$. Dispersion in the thicker QWPC adds a small, overall offset. Set S3 shows the most sensitivity at approximately 0°, but with both SI and S3, the spectral shift disappears at ±45°. If the pulse BW is less than or equal to the QWP range, the spectral shift generally amounts to less than 1 nm. However, for broader BWs, spectral shifts of up to 15 nm are observed for set S1 when QWPC is set to transmit linear polarization (i.e., $\theta = \pm 90°, 0°$). Such large differences in the expected and actual SHG peak locations could easily affect SHG measurements adversely by reducing or even eliminating the detected response for these orientations, depending on the detector's range (for instance, an interference filter with a BW of ±10 nm would reject a significant part, and would certainly lead to polarization-dependent errors in the measured signal, of Sl-type SHG responses at −90°, 0°, and+90°).

Another serious consequence of crystal misalignment is the introduction of an artificial SHCD to the total SHG response for the achiral set S1, in the form of an intensity difference between $\theta = 45°$ and 135° (recall that high-quality CP cannot be obtained with a misaligned QWPC). This result means that an achiral sample, which should exhibit no such difference, could be misidentified as being chiral.[36,37] Figure 10 shows this artificial SHCD for two different thicknesses of a 3°-misaligned QWPC. Interestingly, the thinner QWPC exhibits a larger SHCD (~6%) and angular shift of the total response from the reference. The greater dispersion in the thicker QWPC apparently helps mitigate errors with this set and leads to more effective sideband compensation. Set S2 appears immune to artificial SHCD, while for set S3 the total SHG response develops slight asymmetric tilts at the peaks, most likely the result of competition with the existing chiral signature. Unlike with QWPM, the intentional SHCD is not diminished here. However, the angular shifts in S2 and S3 are exacerbated, not compensated, by thickness, indicating that the polarization behavior of such complicated configurations can be unpredictable, and therefore a misaligned QWP should not be used in chiral measurements. However, distortions are not substantial provided the misalignment is less than $\alpha = 0.5°$.

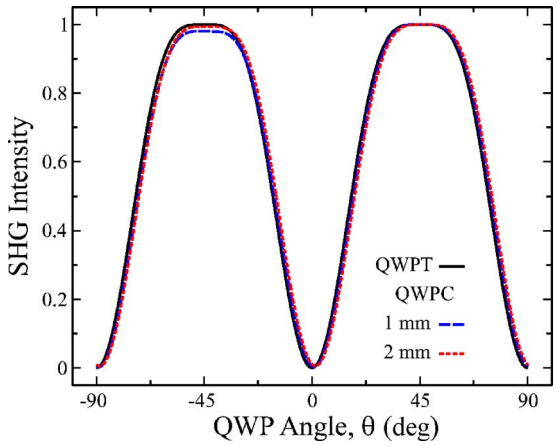

Fig. 10. (Color online) Normalized total SHG responses generated from coefficient set S1 with QWPT, BW1 and 3° misaligned QWPC, BW4 for thicknesses of 1 and 2 mm.

6. CONCLUSION

The broad spectral width of an ultrashort fs pulse can lead to significant adverse polarization modifications upon transmission through a QWP, which in turn affect the SHG response. Dispersion of birefringence in quartz and the specified tolerance limit the BW that even a true zero-order QWP can transmit with nearly nominal retardation. A misalignment of only 1° to 2° between the crystal axes in a compound QWP induces serious, unpredictable distortions to the retardation of frequency modes in the pulse, and good CP becomes unachievable. The acceptance range of the QWP shrinks and shifts away from the design wavelength, and the phase shift between the polarization components no longer depends linearly on frequency. Greater thickness, coupled with misalignment, is more detrimental to the transmitted fundamental polarization, possibly even shifting the QWP range so far that the design wavelength is excluded. A multiorder QWP, having a highly reduced usable range because of dispersion, modifies BB fundamental pulses in a highly undesirable manner.

Deviations in the polarization of a fundamental fs pulse naturally affect the SHG response produced with it. However, the BB nature of the pulse means that the sidebands interact through SFG processes and compensation of polarization errors results. The SHG responses at individual frequencies in the sidebands differ with a true zero-order QWP when the pulse BW exceeds its range, yet for all samples the total SHG response, including sideband SFG contributions, exactly reproduce the ideal responses generated with a narrowband pulse. In the case of the multiorder QWP, good sideband compensation occurs if the pulse BW does not strongly overlap neighboring acceptance bands.

Crystal axis misalignment causes the SHG spectrum to shift away from the central frequency because of different coupling efficiencies of the sideband modes. Small shifts occur even with a true zero-order QWP for a very broad BW, although with a misaligned compound QWP, the shift can be an order of magnitude greater. Such spectral shifts may inhibit or lead to errors in SHG signal detection. Another serious consequence of misalignment is the appearance of an artificial chiral signature, which can lead to erroneous data interpretation. Thickness and misalignment generally work together to increase the deviation of the total SHG response from ideal. Interestingly, though, for certain achiral sample types, dispersion in a thicker QWP appears to compete against misalignment, bringing the total response back in line with the ideal response. This shows the unpredictable nature of the complex polarization behavior resulting from such imperfect optics.

Our results suggest that for the cases of single-crystal and aligned compound WPs, the SHG techniques based on continuous polarization variation with a QWP tolerate polarization errors provided that the laser source BW lies within the 5° phase error range of the QWP. Crystal axis misalignment in a compound WP, on the other hand, is a critical issue: the axes of the two crystals should be aligned with each other to better than 0.5° for reliable results. Thus, in BB-SHG experiments the QWP sets clear limits on the accuracy of a measurement.

ACKNOWLEDGMENTS

K. Laiho is now with the Max-Planck Junior Research Group in Erlangen, Germany. This work was funded by grants 53961 and 54019 from the Finnish Academy.

B. K. Canfield's e-mail address is brian.canfield@tut.fi.

REFERENCES

1. See, for instance, the special issue on femtochemistry, J. Phys. Chem. **97**, 12460–12465 (1993). Includes the major paper by A. Zewail, who won the 1999 Nobel in chemistry for time-resolved studies of molecular interactions.
2. J. J. Macklin, J. D. Kmetec, and C. L. I. Gordon, "High-order harmonic generation using intense femtosecond pulses," Phys. Rev. Lett. **70**, 766–769 (1993).
3. A. M. Malvezzi, M. Allione, M. Patrini, A. Stella, P. Cheyssac, and R. Kofman, "Melting-induced enhancement of the second-harmonic generation from metal nanoparticles," Phys. Rev. Lett. **89**, 087401 (2002).
4. T. Atay, J.-H. Song, and A. V. Nurmikko, "Strongly interacting plasmon nanoparticle pairs: from dipole-dipole interaction to conductively coupled regime," Nano Lett. **4**, 1627–1631 (2004).
5. W. Huang, W. Qian, and M. A. El-Sayed, "Photothermal reshaping of prismatic Au nanoparticles in periodic monolayer arrays by femtosecond laser pulses," J. Appl. Phys. **98**, 114301 (2005).
6. B. Lamprecht, A. Leitner, and F. R. Aussenegg, "SHG studies of plasmon dephasing in nanoparticles," Appl. Phys. B **68**, 419–423 (1999).
7. C. Anceau, S. Brasselet, J. Zyss, and P. Gadenne, "Local second-harmonic generation enhancement on gold nanostructures probed by two-photon microscopy," Opt. Lett. **28**, 713–715 (2003).
8. B. K. Canfield, S. Kujala, M. Kauranen, K. Jefimovs, T. Vallius, and J. Turunen, "Remarkable polarization sensitivity of gold nanoparticle arrays," Appl. Phys. Lett. **86**, 183109 (2005).
9. A. E. Siegman, *Lasers* (University Science Books, 1986).
10. I. V. Tomov, R. Fedosejevs, and A. A. Offenberger, "Up-Conversion of subpicosecond light pulses," IEEE J. Quantum Electron. **18**, 2048–2056 (1982).
11. T. R. Zhang, H. R. Choo, and M. C. Downer, "Phase and group velocity matching for second harmonic generation of femtosecond pulses," Appl. Opt. **29**, 3927–3933 (1990).
12. R. A. Cheville, M. T. Reiten, and N. J. Halas, "Wide-bandwidth frequency doubling with high conversion efficiency," Opt. Lett. **17**, 1343–1345 (1992).
13. H. Zhu, T. Wang, W. Zheng, P. Yuan, L. Qian, and D. Fan, "Efficient second harmonic generation of femtosecond laser at 1 μm," Opt. Express **12**, 2150–2155 (2004).
14. X. Xiao, C. Yang, S. Gao, and H. Miao, "Analysis of ultrashort-pulse second-harmonic generation in both phase- and group-velocity-matched structures," IEEE J. Quantum Electron. **41**, 85–93 (2005).
15. T. Hofmann, K. Mossavi, F. K. Tittel, and G. Szabó, "Spectrally compensated sum-frequency mixing scheme for generation of broadband radiation at 193 nm," Opt. Lett. **17**, 1691–1693 (1992).
16. C. Radzewicz, J. S. Krasinski, and Y. B Band, "Increased efficiency for sumfrequency generation for broadband input fields," Opt. Lett. **18**, 331–333 (1993).
17. K. Osvay and I. N. Ross, "Broadband sum-frequency generation by chirp-assisted group-velocity matching," J. Opt. Soc. Am. B **13**, 1431–1438 (1996).
18. C. J. Sun and J. T. Lue, "Second harmonic generation with focused broad-band and high-order transverse mode lasers," IEEE J. Quantum Electron. **24**, 113–117 (1988).
19. Y. B. Band, D. F. Heller, J. R. Ackerhalt, and J. S. Krasinski, "Spectrum of second-harmonic generation for multimode fields," Phys. Rev. A **42**, 1515—1521 (1990).
20. F. Krausz, M. E. Fermann, T. Brabec, P. F. Curley, M. Hofer, M. H. Ober, C. Spielmann, E. Wintner, and A. J. Schmidt, "Femtosecond solid-state lasers," IEEE J. Quantum Electron. **28**, 2097–2122 (1992).
21. J. O. White, D. Hulin, M. Joffre, A. Migus, A. Antonetti, E. Toussaere, R. Hierle, and J. Zyss, "Ultrabroadband second-harmonic generation in organic and inorganic thin crystals," Appl. Phys. Lett. **64**, 264–266 (1994).
22. E. Sidick, A. Knoesen, and A. Dienes, "Ultrashort-pulse second-harmonic generation. I. Transform-limited fundamental pulses," J. Opt. Soc. Am. B **12**, 1704–1712 (1995).
23. E. Sidick, A. Dienes, and A. Knoesen, "Ultrashort-pulse second-harmonic generation. II. Non-transform-limited fundamental pulses," J. Opt. Soc. Am. B **12**, 1713–1722 (1995).
24. M. Mlejnek, E. M. Wright, J. V. Moloney, and N. Bloembergen, "Second harmonic generation of femtosecond pulses at the boundary of a nonlinear dielectric," Phys. Rev. Lett. **83**, 2934–2937 (1999).
25. R. W. Boyd, *Nonlinear Optics* (Academic, 1992).
26. V. Pasiskevicius, S. J. Holmgren, S. Wang, and F. Laurell, "Simultaneous second-harmonic generation with two orthogonal polarization states in periodically poled KTP," Opt. Lett. **27**, 1628–1630 (2002).
27. R. A. Ganeev, A. Ishizawa, T. Kanai, T. Ozaki, and H. Kuroda, "Polarization peculiarities of femtosecond laser induced harmonic generation from solid surface plasma," Opt. Commun. **227**, 175–182 (2003).
28. D. Hovhannisyan, K. Stepanyan, and R. Avagyan, "Sum and difference frequency generation by femtosecond laser pulses in a nonlinear crystal," Opt. Commun. **245**, 443–456 (2005).
29. M. H. Smith, "Polarization metrology moves beyond 'home-brewed' solutions," Laser Focus World **40**, 123–129 (2004).
30. Selected manufacturers' wave-plate specifications can be found at Casix (http://www.casix.com), CVI (http://www.cvilaser.com), Ekspla (http://www.ekspla.com), and Elan (http://www.elan.spb.ru).
31. E. A. West and M. H. Smith, "Polarization errors associated with birefringent waveplates," Opt. Eng. **34**, 1574–1580 (1995).
32. B. Boulbry, B. L. Jeune, F. Pellen, J. Cariou, and J. Lotrian, "Identification of error parameters and calibration of a double-crystal birefringent wave plate with a broadband spectral light source," J. Phys. D **35**, 2508–2515 (2002).
33. P. D. Hale and G. W. Day, "Stability of birefringent linear retarders (wave plates)," Appl. Opt. **27**, 5146–5153 (1988).
34. L. D. Acquisto, G. Petrucci, and B. Zuccarello, "Full field automated evaluation of the quarter wave plate retardation by phase stepping technique," Opt. Lasers Eng. **37**, 389–400 (2002).
35. S. Cattaneo and M. Kauranen, "Application of second-harmonic generation to retardation measurements," J. Opt. Soc. Am. B **20**, 520–528 (2003).
36. J. J. Maki, M. Kauranen, and A. Persoons, "Surface second-harmonic generation from chiral materials," Phys. Rev. B **51**, 1425–1434 (1995).
37. M. Kauranen, T. Verbiest, S. V. Elshocht, and A. Persoons, "Chirality in surface nonlinear optics," Opt. Mater. **9**, 286–294 (1998).
38. B. K. Canfield, S. Kujala, K. Laiho, K. Jefimovs, J. Turunen, and M. Kauranen, "Chirality arising from small defects in gold nanoparticle arrays," Opt. Express **14**, 950–955 (2006).
39. M. Born and E. Wolf, *Principles of Optics*, Seventh ed. (Cambridge U. Press, 1999).
40. D. Goldstein, *Polarized Light*, 2nd ed. (Dekker, 2003).
41. B. K. Canfield, S. Kujala, K. Jefimovs, Y. Svirko, J. Turunen, and M. Kauranen, "A macroscopic formalism to describe the second-order nonlinear optical response of nanostructures," J. Opt. A, Pure Appl. Opt. **8**, 278–284 (2006).
42. W. H. Glenn, "Second-harmonic generation by picosecond optical pulses," IEEE J. Quantum Electron. **5**, 284–290 (1969).
43. Y. Nabekawa and K. Midorikawa, "Broadband sum

frequency mixing using noncollinear angularly dispersed geometry for indirect phase control of sub-20-femtosecond UV pulses," Opt. Express **11**, 324–338 (2003).
44. The dispersion of crystal quartz was obtained from http://www.cvilaser.com/Common/PDFs/Dispersion_Equations.pdf. Note: Because this URL is too long for the printed column, the reader will need to type it into his or her browser directly.
45. C. F. Bohren and D. R. Huffman, *Absorption and Scattering of Light by Small Particles* (Wiley, 1998).
46. N. H. Burnett, C. Kan, and P. B. Corkum, "Ellipticity and polarization effects in harmonic generation in ionizing neon," Phys. Rev. A **51**, 3418–3121 (1995).
47. K. D. Singer, M. G. Kuzyk, and J. E. Sohn, "Second-order nonlinear-optical processes in orientationally ordered materials: relationship between molecular and macroscopic properties," J. Opt. Soc. Am. B **4**, 968-976 (1987).